Received: 6 July 2020 | Revised: 1 August 2020 | Accepted: 2 August 2020
DOI: 10.1002/aoc.5980

FULL PAPER

Applied Organometallic Chemistry WILEY

Insights into crystal structures, supramolecular architectures and antioxidant activities of self-assembled fluorescent hetero-multinuclear [Cu (II)-Ln (III)] (Ln = La, Ce, Pr and Nd) salamo-like complexes

Lu-Mei Pu[1] | **Xiao-Xin An**[2] | **Chang Liu**[2] | **Hai-Tao Long**[1] | **Li Zhao**[2]

[1]College of Science, Gansu Agricultural University, Lanzhou, Gansu, 730070, China

[2]School of Chemical and Biological Engineering, Lanzhou Jiaotong University, Lanzhou, Gansu, 730070, China

Correspondence
Li Zhao, School of Chemical and Biological Engineering, Lanzhou Jiaotong University, Lanzhou 730070, China.
Email: zhaol@mail.lzjtu.cn

Funding information
Program for Excellent Team of Scientific Research in Lanzhou Jiaotong University, Grant/Award Number: 201706; Science and Technology Program of Gansu Province, Grant/Award Number: 18YF1GA057; National Natural Science Foundation of China, Grant/Award Number: 21761018

Newly designed hetero-dinuclear 3d–4f complex [Cu(L)La $(NO_3)_2(\mu\text{-}NO_3)(H_2O)]\cdot$EtOH (**1**), hetero-tetranuclear 3d–4f complex [Cu(L)Ce $(NO_3)_2(\mu\text{-}NO_3)(OAc)_2]_2\cdot$MeOH (**2**) and hetero-multinuclear 3d–4f complexes [{Cu(L)Ln $(NO_3)_3\}_2$][Cu(L)Ln $(NO_3)_3]_2$ (Ln = Pr (**3**) and Nd = (**4**)) have been self-assembled from the reaction of Cu $(OAc)_2\cdot H_2O$, Ln $(NO_3)_3\cdot 6H_2O$ (Ln = La, Ce, Pr and Nd) with an unsymmetric salamo-like bisoxime ligand H_2L (6-Methoxy-6′-ethoxy-2,2′-[ethylenedioxybis (nitrilomethylidyne)]diphenol) based on a Schiff base condensation of 2-[*O*-(1-ethoxyamide)]oxime-6-methoxyphenol and 3-ethoxysalicylaldehyde. The structures of complexes **1**–**4** were characterized by elemental analyses, PXRD analyses, IR, UV–Vis spectra, and single-crystal X-ray analyses. In addition, the supramolecular interactions and fluorescence properties of complexes **1–4** are discussed in detail. Moreover, the antioxidant activities of the complexes **1–4** were determined by superoxide radical-scavenging method in vitro, which indicates that the complexes **1–4** all show potential antioxidant properties.

KEYWORDS
crystal structure, hetero-multinuclear 3d-4f complex, property, Salamo-like bisoxime ligand, synthesis

1 | INTRODUCTION

Nowadays, the development of coordination chemistry[1–5] has become an important content of modern inorganic chemistry, especially with the help of modern structure theory and modern physical experiment method, it has become a cross subject with rich content, wide range and strong permeability.[6–12] Rare earth, as an indispensable key material in modern society, has attracted more and more attention due to its scarcity of output and value.[13,14]] In recent years, in the research and development of functional materials, the introduction of rare earth elements with unique 4f electronic layer structure and unique physical and chemical properties has been widely developed at home and abroad, and has made great progress, which have open novel possibilities for a broad range of advanced applications, such as electrochemistry,[15–18] supramolecular buildings,[2,19–23] catalysis fields,[24–26] magnetism,[27–31] biological systems,[32–34] chemical sensors,[35–40] luminescence materials,[41–45] and DFT calculations.[46–48] Recently, many novel structural 3d–4f complexes have been reported by using salen-like and salamo-like N_2O_2-donor ligands, which also attracted people's attentions.[5] Excessive accumulation of oxygen free radicals in the cells will have an adverse effect on the body, which is also one of the important factors leading to inflammation and aging. Although natural SOD has excellent scavenging properties for superoxide anion free radicals (O_2•-), its extraction process is complicated, costly, and easily deactivated, so its application is limited. Therefore, the preparation of simulated enzymes capable of scavenging various reactive oxygen radicals has become a research hotspot. In the past decade, their biological activity and many other applications have caused a strong interest in metal complexes.[49–51]

Herein, we designed and synthesized a hexadentate salamo-like bisoxime ligand H_2L (6-Methoxy-6′-ethoxy-2,2′-[ethylenedioxybis (nitrilomethylidyne)]diphenol) with a flexible linker as the electron donor of the formation new complexes. The metal ions provide empty orbits (Cu $(OAc)_2 \cdot H_2O$, Ln $(NO_3)_3 \cdot 6H_2O$ (Ln = La, Ce, Pr and Nd)), which meets the prerequisites for efficient metal complex design. A total of three coordination modes of 3d–4f metal complexes are given in this paper. While discussing the supramolecular interactions of complexes **1–4**, the fluorescence properties were also discussed. In addition, the antioxidant activities of the complexes **1–4** were determined by superoxide anion free radicals scavenging methods in vitro.

2 | RESULTS AND DISCUSSION

2.1 | PXRD analyses

The powder X-ray diffraction (PXRD) patterns of complexes **1–4** are shown in Figure 1. The PXRD experiments were performed on complexes **1–4** using an X-ray diffractometer using Cu-Kα radiation (λ = 0.15406 nm) in the range of 2θ = 5–50°. Its patterns are from single crystal X-ray data of complexes **1–4**. The experimental spectra are in good agreement with the simulated spectra, confirming the phase purity and isomorphism of complexes **1–4**.

2.2 | IR spectra

The strong characteristic absorption peaks of complexes **1–4** in the range of 4,000–400 cm^{-1} were collected in the FT-IR spectra (Figure 2). The phenolic hydroxyl O–H stretching vibrational absorption peak of the ligand H_2L appeared at a large broad peak at *ca.* 3424 cm^{-1}, this band were disappeared in the FT-IR

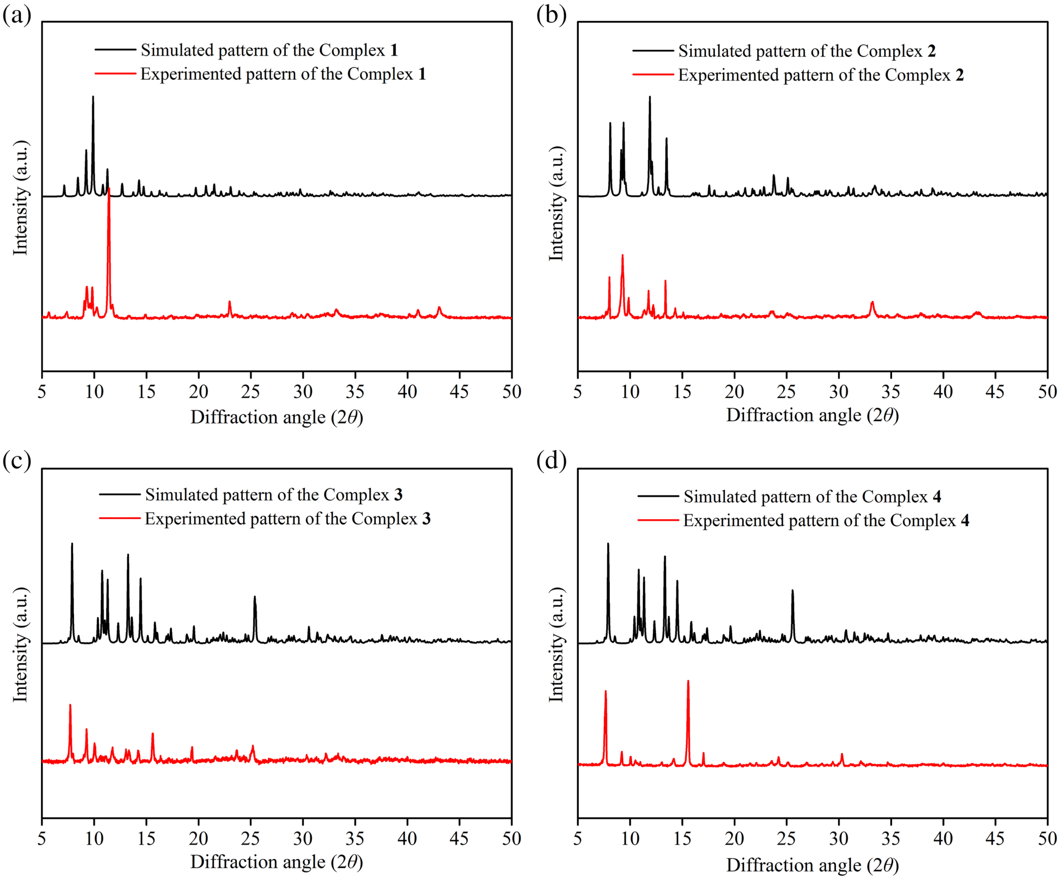

FIGURE 1 Comparison of the simulated and experimental powder X-ray diffraction (PXRD) patterns of the complexes **1–4**: Complex **1** (a); Complex **2** (b); Complex **3** (c); Complex **4** (d)

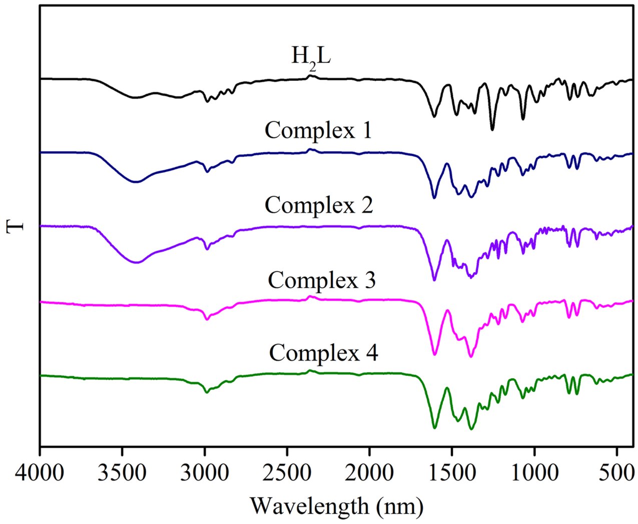

FIGURE 2 IR spectra of H_2L and its complexes **1–4**

spectra of complexes **3** and **4**, which is indicative of the fact that the phenolic hydroxyl groups of the ligand H_2L had been completely deprotonated and coordinated to the M (II/III) atoms.[22,35–37] Besides, complex **1** appeared at *ca.* 3410 cm^{-1} compared to the ligand H_2L, the strong O–H stretching vibration absorption peak belongs to the O–H absorption peak on the free ethanol molecule, while the strong O–H stretching vibration absorption peak in complexe **2** were observed at *ca.* 3407 cm^{-1}, which is attributed to the O–H absorption peak on the free methanol molecules.[10,52] In addition, the ligand H_2L has a typical Ar–O stretching frequency at *ca.* 1250 cm^{-1}, while the Ar–O stretching frequencies in complexes **1–4** were observed at *ca.* 1287, 1,213, 1,216, and 1,232 cm^{-1}, respectively, indicating that Cu–O or Ln–O bonds were formed between the phenol oxygen atoms and the metal (II/III) atoms.[11] Meanwhile, the absorption peak at *ca.* 1610 cm^{-1} was the stretching vibration absorption peak of the C=N bonds of the ligand, while the absorption peaks of the C=N bonds in complexes **1–4** were found at *ca.* 1608, 1,609, 1,606 and 1,607 cm^{-1}, respectively, indicating that the oxime nitrogen atoms of the ligand were coordinated with the Cu (II) atoms.[22,24] The absorption bands of the coordinated nitrate groups were observed at about 1,458–1,467 cm^{-1} (ν_1) and 1,282–1,286 cm^{-1} (ν_4) for the complexes **1–4**, respectively. The differences between the strongest absorption band ν_1 and ν_4 of nitrate groups lie in *ca.* 175–181 cm^{-1},[[53]] indicate the coordinated nitrate groups in the complexes **1–4** are bidentate ligands, which is consistent with the results obtained by X-ray single crystal diffraction.

2.3 | UV–vis absorption spectra

The UV-Vis absorption spectra of H_2L and its complexes **1–4** in ethanol solution are shown in Figure 3a. H_2L has two relatively strong absorption peaks at *ca.* 270 and 319 nm, which are attributed to the π–π* transitions[54,55] of the benzene rings and the C=N bonds in the free ligand H_2L. The UV–Vis spectra of complexes **1–4** are similar but distinct from the ligand, with two absorption peaks around 283 and 350 nm. In the UV–Vis titration experiment, compared with the free ligand H_2L, with the increase of Cu (II) ions, the absorption peaks of the ligand disappeared at *ca.* 270 and 319 nm, because the phenolic oxygen atoms participate in the coordination, which changes the conjugate system of the ligand, and at the same time, new absorption peaks were found at *ca.* 283 and 370 nm. When the addition of Cu (II) ions (1.0×10^{-3} M) was 1.0 equivalent, the coordination end point was reached, indicating that the stoichiometric ratio between Cu (II) ions and H_2L was 1: 1, as shown in Figure 3b. Immediately after the addition of 1.0 equivalent of Ln (III) (La (III), Ce (III), Pr (III) and Nd (III)) ions (1.0×10^{-3} M) (Figure 3c–f), the absorption peak at *ca.* 370 nm gradually disappeared, and new peaks appeared near 350 nm for complexes **1–4**. The results of the titration curve show that the stoichiometric ratio between H_2L: Cu (II): Ln (III) is 1: 1: 1. This result is consistent with the crystal structures obtained by single crystal diffraction.

2.4 | Crystal structure descriptions

Complexes **1–4** were synthesized in CH_2Cl_2 – EtOH or CH_2Cl_2 – MeOH solution of H_2L, Cu $(OAc)_2 \cdot H_2O$ and Ln $(NO_3)_3 \cdot 6H_2O$ in a 1: 1: 1 molar ratio by one-pot method, respectively. The synthetic routes to complexes **1–4** are given in the Figure 4. X-ray crystallographic analysis reveals the crystal structures of complexes **1–4**. A summary of selected bond lengths and angles for complexes **1–4** are given in Table **1**. Hydrogen bonding distances and bond angles for complexes **1–4** are listed in Table **2**.

2.4.1 | Crystal structure of complex 1

The crystal structure of complex **1** was determined by X-ray single-crystal diffraction analysis. Complex **1** crystallizes in the triclinic space group *P* – 1. For complex **1**, the structure is composed of a $[Cu(L)La\ (NO_3)_2(\mu\text{-}NO_3)(H_2O)]$ unit and a crystalline ethanol molecule. As shown in Figure 5, the unique inner Cu (II) atom (Cu1) is five-coordinate and bound by the N_2O_2 (N1, N2, O2 and O5) core of the salamo-like bisoxime ligand $(L)^{2-}$ units in

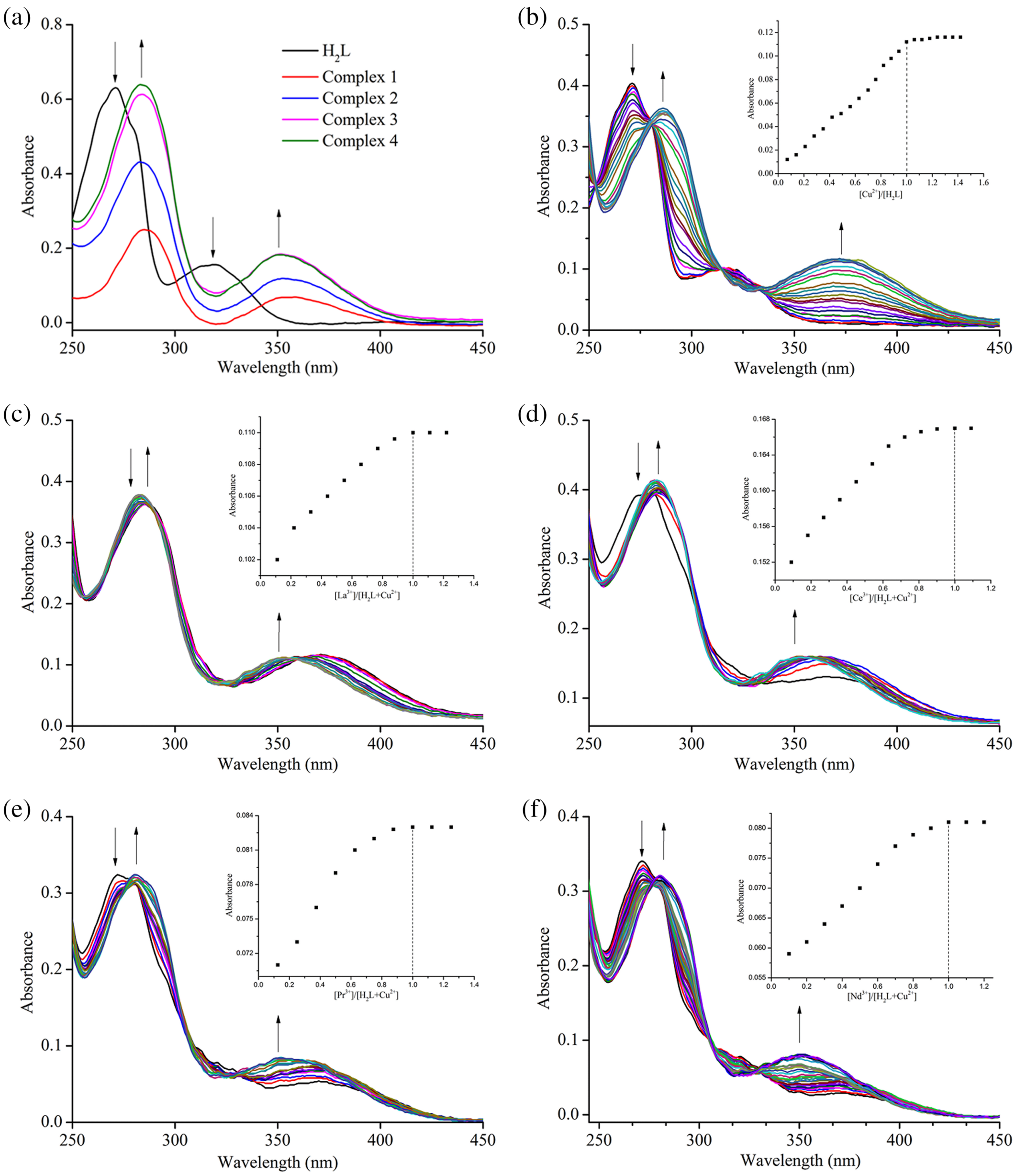

FIGURE 3 The UV–Vis spectra of H_2L and its complexes **1**–**4** in ethanol solutions (1.0×10^{-5} M) (a); The UV–Vis titration spectra of H_2L changes after the addition of Cu $(OAc)_2 \cdot H_2O$ (1.0×10^{-3} M) (b); The UV–Vis titration spectra of $[(L)–Cu^{2+}]$ changes after the addition of La $(NO_3)_3 \cdot 6H_2O$ (c), Ce $(NO_3)_3 \cdot 6H_2O$ (d) Pr $(NO_3)_3 \cdot 6H_2O$ (e) and Nd $(NO_3)_3 \cdot 6H_2O$ (f) (1.0×10^{-3} M)

addition to one oxygen atom (O14) from the bridged nitrate group, it eventually presents an almost square pyramid geometry ($\tau = 0.09317$).[56,57] However, the outer La (III) atom (La1) is ten-coordinated: in addition to the four oxygen atoms from the outer O_4 (O1, O2, O5 and O6) moieties of the salamo-like bisoxime ligands, where four oxygen atoms (O7, O8, O10 and O11) are from two bidentate nitrate groups and two oxygen atoms (O13 and O16) from the bridged nitrate group and the coordinated H_2O molecule, which presume a distorted double-capped tetragonal anti-prism geometry.

Each molecule forms two intramolecular hydrogen bonds (C16–H16A···O10 and C2–H2AB···O10), as shown in Figure 6a. At the same time, a self-assembled infinite two-dimensional supramolecular structure is formed by the interaction of seven intermolecular hydrogen bonds (O16–H16A···O10, O16–H16A···O12, O16–H16B···O4, O17–H17A···O16, O17–H17A···O15, C9–H9···O7 and C12–H12···O7) (Figure 6b). As shown in Figure 6c, the 3D intermolecular structure of complex **1** is given.

2.4.2 | Crystal structure of complex 2

The crystallographic data reveals that complex **2** consists of a crystalline methanol molecule and two hetero-

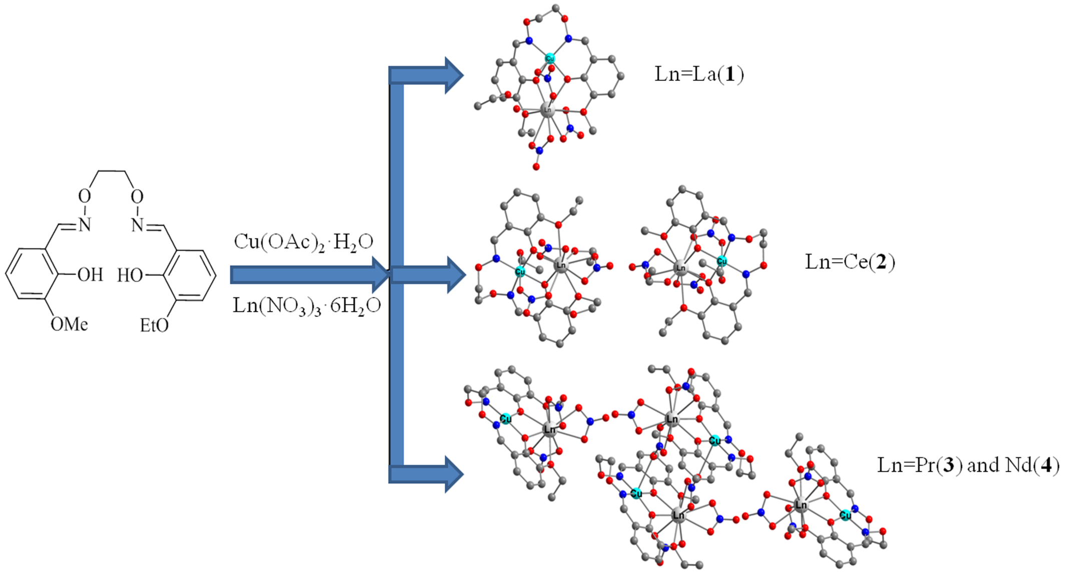

FIGURE 4 Synthetic routes to complexes **1–4**

TABLE 1 Selected bond lengths (Å) and angles (°) for complexes **1–4**

Complex 1					
Bond	**Lengths**	**Bond**	**Lengths**	**Bond**	**Lengths**
La1-O2	2.523(2)	La1-O11	2.601(3)	Cu1-O2	1.943(2)
La1-O5	2.466(2)	La1-O16	2.492(3)	Cu1-O5	1.915(2)
La1-O6	2.726(2)	La1-O7	2.623(3)	Cu1-N2	1.929(3)
La1-O10	2.680(2)	La1-O13	2.627(3)	Cu1-N1	1.979(3)
La1-O1	2.723(2)	La1-O8	2.628(3)	Cu1-O14	2.485(3)
Bond	Angles	Bond	Angles	Bond	Angles
O2-La1-O6	113.96(7)	O11-La1-O6	118.94(8)	O7-La1-O6	24.22(11)
O2-La1-O10	170.58(7)	O11-La1-O10	47.98(8)	O13-La1-O6	148.98(9)
O2-La1-O1	59.55(7)	O11-La1-O1	74.76(8)	O13-La1-O10	110.02(9)
O2-La1-O11	126.38(8)	O11-La1-O7	120.80(10)	O13-La1-O1	70.75(9)
O2-La1-O7	71.16(8)	O11-La1-O13	69.30(9)	O13-La1-O8	131.45(11)
O2-La1-O13	70.25(8)	O11-La1-O8	74.85(11)	O8-La1-O6	77.79(9)
O2-La1-O8	109.49(9)	O16-La1-O2	121.82(9)	O8-La1-O10	62.88(9)
O5-La1-O2	61.65(7)	O16-La1-O6	74.99(9)	O8-La1-O1	68.99(9)
O5-La1-O6	59.64(7)	O16-La1-O10	66.69(9)	O2-Cu1-N1	169.55(11)
O5-La1-O10	126.35(8)	O16-La1-O1	144.98(10)	O5-Cu1-O2	83.02(9)
O5-La1-O1	119.30(7)	O16-La1-O11	80.97(10)	O5-Cu1-N2	163.96(11)
O5-La1-O11	161.42(9)	O16-La1-O7	143.48(10)	O5-Cu1-N1	89.79(11)
O5-La1-O16	80.93(9)	O16-La1-O13	77.28(10)	N2-Cu1-O2	90.28(11)
O5-La1-O7	76.97(9)	O16-La1-O8	128.06(10)	N2-Cu1-N1	98.55(12)
O5-La1-O13	102.50(9)	O7-La1-O6	68.81(9)	O2-Cu1-O14	77.35(10)
O5-La1-O8	120.33(10)	O7-La1-O10	104.59(9)	O5-Cu1-O14	78.83(11)
O10-La1-O6	70.96(8)	O7-La1-O1	71.51(9)	O14-Cu1-N1	93.85(11)
O10-La1-O1	111.31(8)	O7-La1-O13	135.74(10)	O14-Cu1-N2	113.99(13)
O1-La1-O6	139.24(8)	O7-La1-O8	48.13(10)		
Complex **2**					
Bond	Lengths	Bond	Lengths	Bond	Lengths
Ce1-O7	2.525(2)	Ce1-O14	2.515(14)	Cu1-N2	2.006(2)
Ce1-O1	2.6716(18)	Ce1-O10	2.633(2)	Cu1-O17	2.395(2)

(Continues)

TABLE 1 (Continued)

Complex 1					
Bond	**Lengths**	**Bond**	**Lengths**	**Bond**	**Lengths**
Ce1-O11	2.551(2)	Ce1-O13	2.715(9)	Cu1-O5	1.9234(16)
Ce1-O2	2.4904(18)	Ce1-O5	2.4411(16)	Cu1-O8	2.741(3)
Ce1-O16	2.510(2)	Cu1-N1	1.952(2)		
Ce1-O6	2.667(2)	Cu1-O2	1.9771(18)		
Bond	Angles	Bond	Angles	Bond	Angles
O7-Ce1-O1	74.77(7)	O16-Ce1-O11	73.10(8)	O5-Ce1-O16	80.51(7)
O7-Ce1-O11	115.71(7)	O16-Ce1-O6	66.26(7)	O5-Ce1-O6	60.55(6)
O7-Ce1-O6	143.84(7)	O16-Ce1-O14	142.2(2)	O5-Ce1-O14	73.0(3)
O7-Ce1-O10	67.08(7)	O16-Ce1-O10	116.21(7)	O5-Ce1-O10	162.63(7)
O7-Ce1-O13	85.90(19)	O16-Ce1-O13	125.51(19)	O5-Ce1-O13	107.9(2)
O1-Ce1-O13	129.4(2)	O6-Ce1-O1	141.24(7)	N1-Cu1-O2	89.88(8)
O11-Ce1-O1	78.91(7)	O6-Ce1-O13	72.10(19)	N1-Cu1-N2	99.29(9)
O11-Ce1-O6	82.81(7)	O14-Ce1-O7	67.1(3)	N1-Cu1-O17	89.79(9)
O11-Ce1-O10	48.87(7)	O14-Ce1-O1	141.5(2)	O2-Cu1-N2	162.57(8)
O11-Ce1-O13	68.2(2)	O14-Ce1-O11	112.9(3)	O2-Cu1-O17	105.57(8)
O2-Ce1-O7	74.38(6)	O14-Ce1-O6	77.2(2)	N2-Cu1-O17	89.36(9)
O2-Ce1-O1	61.17(6)	O14-Ce1-O10	90.0(3)	O5-Cu1-N1	170.66(8)
O2-Ce1-O11	135.20(7)	O14-Ce1-O13	44.7(4)	O5-Cu1-O2	81.19(7)
O2-Ce1-O16	77.84(7)	O10-Ce1-O1	70.01(7)	O5-Cu1-N2	90.04(8)
O2-Ce1-O6	115.40(6)	O10-Ce1-O6	120.06(7)	O5-Cu1-O17	90.00(8)
O2-Ce1-O14	111.1(3)	O10-Ce1-O13	59.4(2)	O2-Cu1-O8	76.39(7)
O2-Ce1-O10	123.72(7)	O5-Ce1-O7	101.95(6)	O5-Cu1-O8	85.78(8)
O2-Ce1-O13	154.4(2)	O5-Ce1-O1	121.55(6)	O8-Cu1-O17	175.06(8)
O16-Ce1-O7	146.59(8)	O5-Ce1-O11	141.30(7)	O8-Cu1-N1	94.79(9)
O16-Ce1-O1	75.78(7)	O5-Ce1-O2	61.95(6)	O8-Cu1-N2	88.04(9)
Complex **3**					
Bond	Lengths	Bond	Lengths	Bond	Lengths
Pr1-O5	2.428(3)	Pr2-O16	2.448(3)	Cu1-O5	1.919(3)
Pr1-O2	2.465(3)	Pr2-O19	2.423(3)	Cu1-O5	1.927(3)
Pr1-O6	2.565(3)	Pr2-O26	2.538(4)	Cu1-N1	1.941(3)
Pr1-O9	2.608(3)	Pr2-O15	2.564(3)	Cu1-N2	1.988(3)
Pr1-O6AA	2.572(3)	Pr2-O20	2.536(5)	Cu2-O16	1.929(3)
Pr1-O11	2.544(3)	Pr2-O28	2.566(4)	Cu2-O19	1.920(3)
Pr1-O8	2.563(3)	Pr2-O22	2.578(4)	Cu2-N6	1.931(4)
Pr1-O1	2.562(3)	Pr2-O2AA	2.575(3)	Cu2-N7	1.980(4)
Pr1-O14	2.549(4)	Pr2-O25	2.603(6)	Cu2-O21	2.786(5)
Pr1-O12	2.561(4)	Pr2-O23	2.577(6)		
Bond	Angles	Bond	Angles	Bond	Angles
O5-Pr1-O2	61.68(8)	O14-Pr1-O6AA	75.47(13)	O15-Pr2-O23	103.9(2)
O5-Pr1-O6	76.40(11)	O14-Pr1-O8	145.07(13)	O20-Pr2-O26	136.49(18)
O5-Pr1-O9	130.43(12)	O14-Pr1-O1	78.20(12)	O20-Pr2-O15	131.02(14)
O5-Pr1-O6AA	62.66(9)	O14-Pr1-O12	49.31(14)	O20-Pr2-O28	143.50(16)
O5-Pr1-O11	141.94(10)	O12-Pr1-O6	160.80(14)	O20-Pr2-O22	48.02(14)
O5-Pr1-O8	74.10(11)	O12-Pr1-O9	67.35(14)	O20-Pr2-O2AA	73.29(14)
O5-Pr1-O1	123.56(9)	O12-Pr1-O6AA	78.42(12)	O20-Pr2-O25	74.9(2)
O5-Pr1-O14	79.91(11)	O12-Pr1-O8	132.55(13)	O20-Pr2-O23	72.0(2)
O5-Pr1-O12	122.71(13)	O12-Pr1-O1	75.62(12)	O28-Pr2-O22	148.00(17)
O2-Pr1-O6	70.86(11)	O16-Pr2-O26	111.79(15)	O28-Pr2-O2AA	75.02(14)
O2-Pr1-O9	165.59(11)	O16-Pr2-O15	62.47(11)	O28-Pr2-O25	137.5(2)
O2-Pr1-O6AA	119.65(9)	O16-Pr2-O20	110.58(15)	O28-Pr2-O23	115.9(2)
O2-Pr1-O11	116.92(10)	O16-Pr2-O28	71.69(13)	O22-Pr2-O25	64.2(2)

TABLE 1 (Continued)

Complex 1					
Bond	**Lengths**	**Bond**	**Lengths**	**Bond**	**Lengths**
O2-Pr1-O8	112.05(11)	O16-Pr2-O22	76.59(14)	O2AA-Pr2-O22	119.76(13)
O2-Pr1-O1	62.40(9)	O16-Cu1-O2AA	120.99(11)	O2AA -Pr2-O25	117.97(16)
O2-Pr1-O14	73.79(13)	O16-Cu1-O25	119.65(16)	O2AA -Pr2-O23	74.50(19)
O2-Pr1-O12	114.70(12)	O16-Cu1-O23	164.51(18)	O23-Pr2-O22	95.9(2)
O6-Pr1-O9	102.64(12)	O19-Pr2-O16	61.94(11)	O23-Pr2-O25	45.3(2)
O6-Pr1-O6AA	115.78(11)	O19-Pr2-O26	117.27(15)	O5-Cu1-O2	81.41(11)
O6AA-Pr1-O9	74.70(11)	O19-Pr2-O15	124.10(11)	O5-Cu1-N1	167.39(13)
O11-Pr1-O6	68.52(11)	O19-Pr2-O20	75.39(16)	O5-Cu1-N2	90.07(12)
O11-Pr1-O9	49.09(11)	O19-Pr2-O28	74.36(14)	O2-Cu1-N1	90.96(13)
O11-Pr1-O6AA	120.79(10)	O19-Pr2-O22	87.30(17)	O2-Cu1-N2	165.86(13)
O11-Pr1-O8	72.15(11)	O19-Cu1-O2AA	62.90(12)	N1-Cu1-N2	99.27(14)
O11-Pr1-O1	73.37(10)	O19-Cu1-O25	148.13(19)	O16-Cu2-N6	90.80(16)
O11-Pr1-O14	137.97(12)	O19-Cu1-O23	132.0(2)	O16-Cu2-N7	169.44(15)
O11-Pr1-O12	93.37(13)	O26-Pr2-O15	78.79(15)	O19-Cu2-O16	81.26(13)
O8-Pr1-O6	49.55(12)	O26-Pr2-O28	48.91(15)	O19-Cu2-N6	164.29(16)
O8-Pr1-O9	69.49(14)	O26-Pr2-O22	155.33(18)	O19-Cu2-N7	91.47(17)
O8-Pr1-O6AA	72.04(11)	O26-Pr2-O2AA	76.96(15)	N6-Cu2-N7	98.01(19)
O1-Pr1-O6	92.46(11)	O26-Pr2-O25	92.4(2)	O21-Cu2-N6	80.28(18)
O1-Pr1-O9	106.00(13)	O26-Pr2-O23	69.9(2)	O19-Cu2-O21	111.01(17)
O1-Pr1-O6AA	151.18(11)	O15-Pr2-O28	83.53(14)	O16-Cu2-O21	78.32(15)
O1-Pr1-O8	136.01(11)	O15-Pr2-O22	85.58(14)	O21-Cu2-N7	97.36(19)
O14-Pr1-O6	143.69(13)	O15-Pr2-O2AA	154.64(12)		
O14-Pr1-O9	113.66(14)	O15-Pr2-O25	70.22(16)		
Complex **4**					
Bond	Lengths	Bond	Lengths	Bond	Lengths
Nd1-O2	2.399(8)	Nd2-O17	2.409(7)	Cu1-O2	1.921(9)
Nd1-O5	2.418(8)	Nd2-O20	2.456(7)	Cu1-O5	1.934(8)
Nd1-O12	2.521(9)	Nd2-O25	2.528(7)	Cu1-N2	1.937(10)
Nd1-O7	2.528(9)	Nd2-O24	2.536(8)	Cu1-N1	1.982(10)
Nd1-O6	2.547(8)	Nd2-O22	2.548(8)	Cu1-O11	2.743(10)
Nd1-O1	2.566(8)	Nd2-O29	2.547(7)	Cu2-O17	1.930(7)
Nd1-O9	2.566(9)	Nd2-O30	2.548(7)	Cu2-O20	1.937(6)
Nd1-O15	2.583(9)	Nd2-O21	2.548(7)	Cu2-N6	1.957(8)
Nd1-O10	2.587(9)	Nd2-O16	2.561(7)	Cu2-N7	1.996(8)
Nd1-O14	2.624(10)	Nd2-O26	2.603(8)		
Bond	Angles	Bond	Angles	Bond	Angles
O2-Nd1-O5	62.1(3)	O2-Nd1-O14	144.1(3)	O30-Nd2-O21	92.6(2)
O2-Nd1-O12	76.4(3)	O5-Nd1-O14	118.3(3)	O17-Nd2-O16	63.2(2)
O5-Nd1-O12	113.3(3)	O12-Nd1-O14	71.1(3)	O20-Nd2-O16	120.6(2)
O2-Nd1-O7	117.9(3)	O7-Nd1-O14	96.0(3)	O25-Nd2-O16	120.4(2)
O2-Nd1-O7	110.9(3)	O6-Nd1-O14	70.7(3)	O24-Nd2-O16	75.7(2)
O12-Nd1-O7	134.8(3)	O1-Nd1-O14	118.7(3)	O22-Nd2-O16	78.3(2)
O2-Nd1-O6	124.7(3)	O9-Nd1-O14	141.2(3)	O29-Nd2-O16	72.0(2)
O5-Nd1-O6	62.8(3)	O15-Nd1-O14	47.7(3)	O30-Nd2-O16	116.1(2)
O12-Nd1-O6	131.4(3)	O10-Nd1-O14	64.6(3)	O21-Nd2-O16	150.9(2)
O7-Nd1-O6	78.2(3)	O17-Nd2-O20	62.2(2)	O17-Nd2-O26	129.5(2)
O2-Nd1-O1	63.5(3)	O17-Nd2-O25	141.4(2)	O20-Nd2-O26	166.0(2)
O5-Nd1-O1	121.0(3)	O20-Nd2-O25	116.5(2)	O25-Nd2-O26	49.9(2)
O12-Nd1-O1	73.1(3)	O17-Nd2-O24	79.9(2)	O24-Nd2-O26	113.9(3)
O7-Nd1-O1	76.6(3)	O20-Nd2-O24	73.5(2)	O22-Nd2-O26	67.1(3)
O6-Nd1-O1	153.9(3)	O25-Nd2-O24	138.5(3)	O29-Nd2-O26	68.6(3)

(Continues)

TABLE 1 (Continued)

Complex 1					
Bond	**Lengths**	**Bond**	**Lengths**	**Bond**	**Lengths**
O2-Nd1-O9	74.6(3)	O17-Nd2-O22	123.3(3)	O30-Nd2-O26	103.4(2)
O5-Nd1-O9	70.9(3)	O20-Nd2-O22	114.8(2)	O21-Nd2-O26	106.3(2)
O12-Nd1-O9	143.6(3)	O25-Nd2-O22	93.3(3)	O16-Nd2-O26	73.4(2)
O7-Nd1-O9	49.1(3)	O24-Nd2-O22	50.1(3)	O2-Cu1-O5	80.2(3)
O6-Nd1-O9	83.9(3)	O17-Nd2-O29	74.3(2)	O2-Cu1-N2	164.7(4)
O1-Nd1-O9	74.5(3)	O20-Nd2-O29	112.8(2)	O5-Cu1-N2	91.5(4)
O2-Nd1-O15	134.1(3)	O25-Nd2-O29	71.5(2)	O2-Cu1-N1	91.7(4)
O5-Nd1-O15	163.4(3)	O24-Nd2-O29	145.2(2)	O5-Cu1-N1	169.6(4)
O12-Nd1-O15	73.2(3)	O22-Nd2-O29	131.9(3)	N2-Cu1-N1	97.8(4)
O7-Nd1-O15	67.0(3)	O17-Nd2-O30	75.8(2)	O11-Cu1-N1	97.2(4)
O6-Nd1-O15	101.1(3)	O20-Nd2-O30	70.3(2)	O5-Cu1-O11	79.7(3)
O1-Nd1-O15	75.2(3)	O25-Nd2-O30	68.7(2)	O2-Cu1-O11	110.3(3)
O9-Nd1-O15	113.6(3)	O24-Nd2-O30	142.7(3)	O11-Cu1-N2	80.5(4)
O2-Nd1-O10	82.8(3)	O22-Nd2-O30	160.7(3)	O17-Cu2-O20	81.2(3)
O5-Nd1-O10	74.7(3)	O29-Nd2-O30	50.2(2)	O17-Cu2-N6	167.3(3)
O12-Nd1-O10	49.1(3)	O17-Nd2-O21	124.2(2)	O20-Cu2-N6	90.5(3)
O7-Nd1-O10	159.1(3)	O20-Nd2-O21	62.5(2)	O17-Cu2-N7	90.3(3)
O6-Nd1-O10	87.4(3)	O25-Nd2-O21	73.2(2)	O20-Cu2-N7	166.0(3)
O1-Nd1-O10	118.7(3)	O24-Nd2-O21	78.2(2)	N6-Cu2-N7	99.6(3)
O9-Nd1-O10	144.7(3)	O22-Nd2-O21	75.2(3)		
O15-Nd1-O10	101.6(3)	O29-Nd2-O21	136.0(2)		

binuclear [Cu(L)Ce $(NO_3)_2(\mu\text{-}NO_3)(OAc)_2]_2$ units that are chemically equivalent and not crystallographically equivalent, crystallizing in the monoclinic system, space group *C*2/c (Figure 7). The Cu (II) atoms with a smaller radius are located in the N_2O_2 cavity of the salamo-like bisoxime ligand $(L)^{2-}$ units, The Ce (III) atoms with larger radius are located in the cavity of O_4 tetradentate mode of $(L)^{2-}$ units, resulting in the formation of the hetero-dinuclear [Cu-Ce-L] host structure. Different from complex **1**, Cu (II) atoms (Cu1) are composed of two oxygen atoms (O2 and O5) and two nitrogen atoms (N1 and N2) from N_2O_2 cavity, one oxygen atom (O8) on a bridged nitrate group and one oxygen atom (O17) on a monodentate acetate group to form six coordination, which is considered as a distorted octahedral geometry. Meanwhile, the Ce (III) atoms (Ce1) are located at the site of the four phenoxy donors (O1, O2, O5 and O6) of the complete deprotonated $(L)^{2-}$ units, in addition to the coordination with the four oxygen atoms of two bidentate nitrate groups (O10, O11, O13 and O14), one oxygen atom of the bridging nitrate group (O7) and one oxygen atom (O16) of monodentate acetate group are also involved in the coordination. The final ten-coordinated Ce (III) atoms possesses a twisted double-capped tetragonal anti-prism geometry.

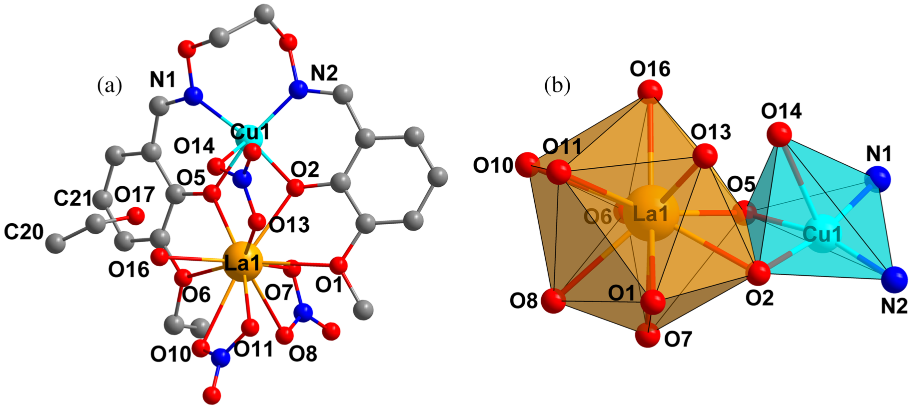

FIGURE 5 (a) Molecule structure of complex **1** (hydrogen atoms are omitted for clarity); (b) Coordination environments for Cu (II) and La (III) atoms

TABLE 2 Hydrogen bonding distances (Å) and bond angles (°) for complexes **1–4**

D–H···A	d(D–H)	d(H···A)	d(D···A)	∠D–H···A	Sum
Complex **1**					
O16–H16A···O10	0.86	2.57	2.848(4)	100	
O16–H16A···O10	0.86	2.43	3.134(4)	139	-x,1-y,1-z
O16–H16A···O12	0.86	2.16	2.964(5)	155	-x,1-y,1-z
O16–H16B···O4	0.86	2.53	3.298(4)	150	1-x,-y,1-z
O17–H17A···O16	0.82	2.31	2.755(5)	114	
O17–H17A···O15	0.82	2.58	2.987(6)	112	1-x,1-y,1-z
C2–H2AB···O10	0.97	2.45	3.164(6)	130	
C9–H9···O17	0.93	2.54	3.319(6)	142	1-x,-y,1-z
C12–H12···O7	0.93	2.27	3.135(5)	155	1-x,-y,2-z
Complex **2**					
O16–H16···O9	0.85(4)	1.95(3)	2.772(3)	165(6)	x,1 + y,z
C17–H17···O9	0.868(17)	1.99(2)	2.801(4)	155(3)	x,1 + y,z
C11–H11A···O3	0.97	2.51	3.475(4)	170	1/2-x,-1/2 + y,1/2-z
C11–H11···O8	0.97	2.59	3.532(4)	163	
C24–H24A···O18	0.96	1.41	2.08(3)	121	-x,y,1/2-z
Complex **3**					
C0AA–H0AA···O23	0.96	2.49	3.142(14)	125	
C4–H4···O22	0.93	2.55	3.408(7)	153	2-x,2-y,-z
C10–H10A···O7	0.97	2.58	3.427(8)	146	1-x,2-y,-z
C10–H10B···O11	0.97	2.58	3.315(7)	132	1-x,2-y,-z
C14–H14···O27	0.93	2.55	3.369(8)	148	-1 + x,y,z
C22–H22···O7	0.93	2.57	3.372(10)	145	1 + x,y,z
C23–H23···O6	0.93	2.58	3.482(7)	163	2-x,2-y,-z
C29–H29A···O21	0.97	2.34	3.300(9)	172	3-x,3-y,1-z
C32–H32···O14	0.93	2.49	3.212(9)	134	2-x,2-y,1-z
C34–H34···O3	0.93	2.57	3.255(7)	131	2-x,2-y,1-z
Complex **4**					
C3–H3···O19	0.95	2.53	3.256(16)	133	1 + x,y,z
C5–H5···O24	0.95	2.45	3.174(18)	133	1 + x,y,z
C9–H9A···O13	0.99	2.56	3.438(19)	147	2-x,-y,1-z
C9–H9B···O11	0.99	2.31	3.30(2)	171	2-x,-y,1-z
C11–H11···O26	0.95	2.48	3.418(17)	169	2-x,1-y,1-z
C14–H14···O30	0.95	2.52	3.430(15)	161	1 + x,y,1 + z
C15–H15···O28	0.95	2.53	3.339(18)	143	1-x,1-y,1-z
C19–H19B···O27	0.98	2.59	3.275(16)	127	1-x,1-y,-z
C22–H22···O10	0.95	2.55	3.408(14)	150	-1 + x,y,-1 + z
C23–H23···O13	0.95	2.56	3.400(18)	148	-x,-y,-z
C28–H28A···O28	0.99	2.53	3.393(15)	145	-x,1-y,-z
C28–H28B···O25	0.99	2.54	3.293(15)	132	-x,1-y,-z
C31–H31···O9	0.95	2.58	3.296(17)	132	-1 + x,y,z
C32–H32···O8	0.95	2.53	3.346(16)	144	1-x,1-y,1-z
C36–H36B···O26	0.99	2.59	3.191(15)	119	
C37–H37C···O15	0.98	2.48	3.15(2)	125	

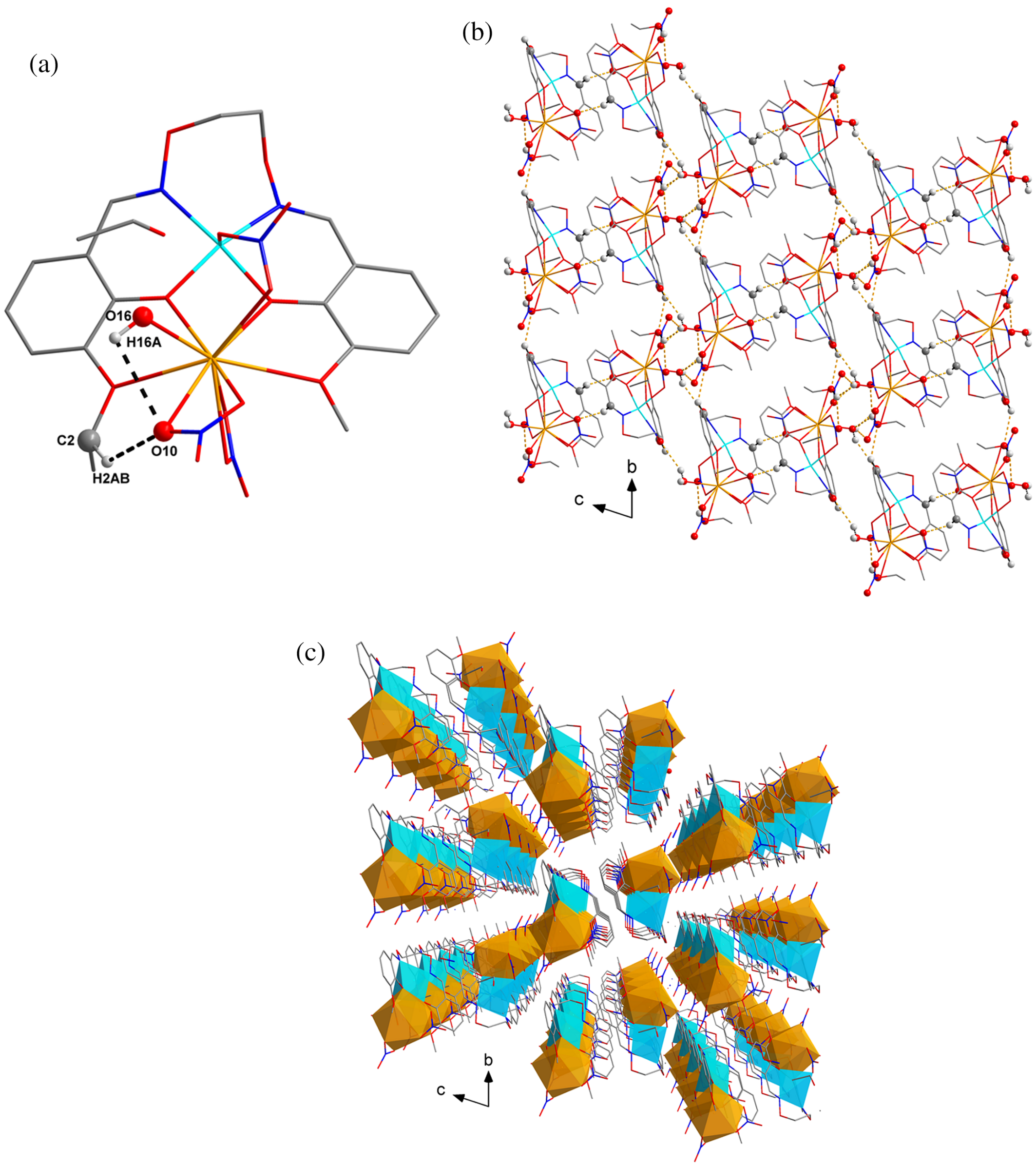

FIGURE 6 (a) View of the intramolecular hydrogen bonding interactions of complex **1**; (b) View of intermolecular hydrogen bonding interactions of complex **1**(hydrogen atoms, except those forming hydrogen bonds, are omitted for clarity); (c) View of the 3D intermolecular structure of complex **1**

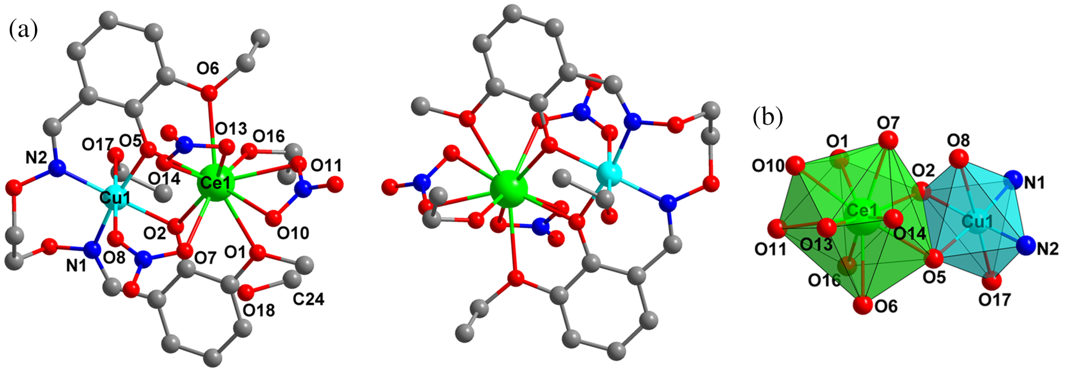

FIGURE 7 (a) Molecule structure of complex **2** (hydrogen atoms are omitted for clarity); (b) Coordination environments for Cu (II) and Ce (III) atoms

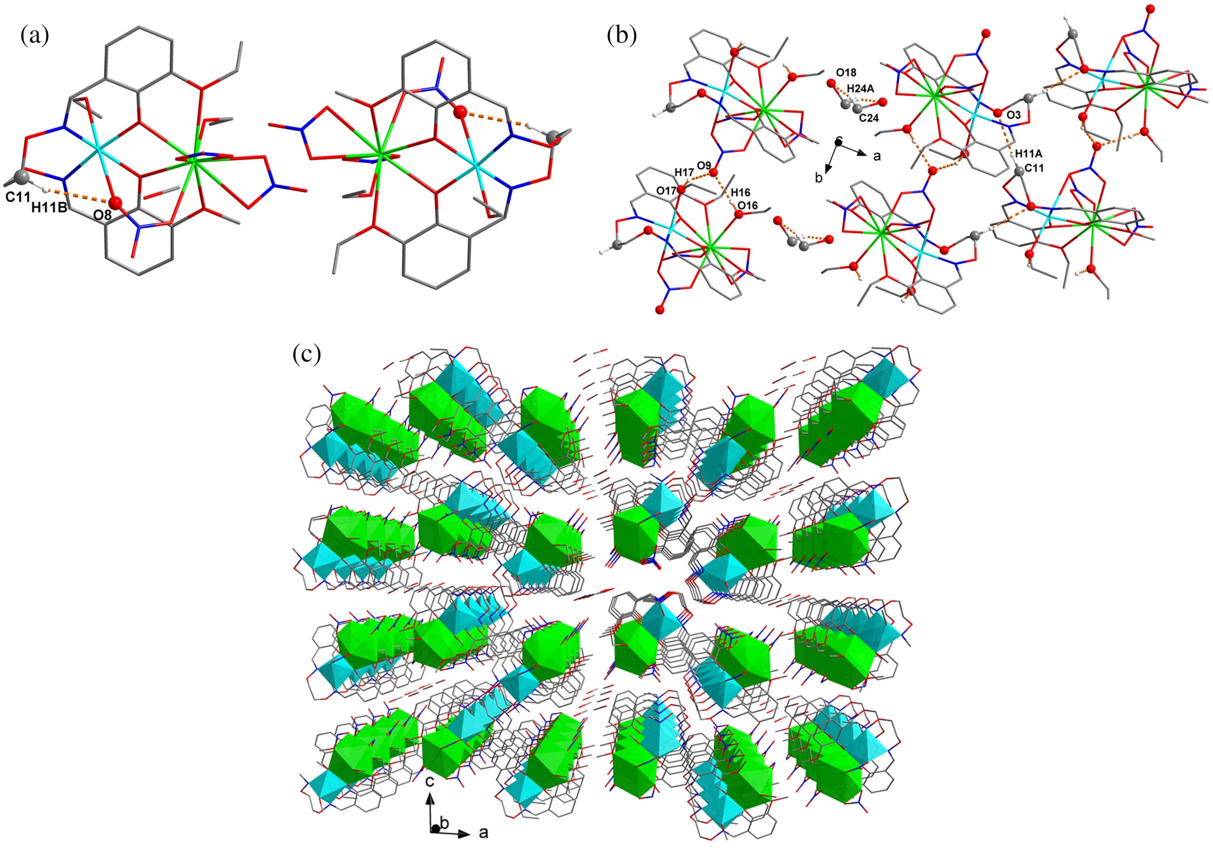

FIGURE 8 (a) View of the intramolecular hydrogen bonding interactions of complex **2**; (b) View of intermolecular hydrogen bonding interactions of complex **2** (hydrogen atoms, except those forming hydrogen bonds, are omitted for clarity); (c) View of the 3D intermolecular structure of complex **2**

As shown in Figure 8a, in the crystal structure of complex **2**, there are only one intramolecular hydrogen bond (C11 – H11B···O8). Moreover, the 2D supramolecular structure is formed by O16 – H16···O9, O17 – H17···O9, C11 – H11A···O3 and C24 – H24A···O18 typical hydrogen bonding interactions in complex **2** (Figure 8b) and finally form a 3D intermolecular structure (Figure 8c).[19–23]

2.4.3 | Crystal structure of complex 3

Complex **3** crystallizes in the triclinic crystal system, space group *P* − 1. X-ray crystallography clearly shows the formation of complex **3**. Unlike complexes **1** and **2**, complex **3** contains one neutral dimer [Cu(L)Pr $(NO_3)_3]_2$ unit and two independent and equivalent [Cu(L)Pr $(NO_3)_3$] units (Figure 9). The Cu (II) atoms in complex **3** have two configurations, while Pr (III) atoms have only one configuration. As shown in Figure 9a, in the independent [Cu(L)Pr $(NO_3)_3$] units, the Cu (II) atoms (Cu1) are only surrounded by two nitrogen atoms (N1 and N2) and two oxygen atoms (O2 and O5) of the ligand $(L)^{2-}$ units form a quadrilateral; in the neutral dimer [Cu(L)Pr $(NO_3)_3]_2$ unit, the Cu (II) atoms (Cu2) are replaced by two nitrogen atoms (N6 and N7) and two oxygen atoms (O16 and O19) from the ligand $(L)^{2-}$ units serves as the equatorial plane, while one oxygen atom (O21) of the bridging nitrate group occupies the apex, and finally forms the geometric configuration of a square pyramid ($\tau = 0.08583$). The Pr (III) atoms (Pr1 and Pr2) in complex **3** are all ten-coordinated, which consists of four oxygen atoms in the ligand $(L)^{2-}$ units and six oxygen atoms from three bidentate chelate nitrate groups. The Pr (III) atoms are also located in the O_{10} site, forming the geometry of a double quadrangular anti-prism geometry. As depicted in Figure 9b, details of the coordination environments of the Cu (II) and Pr (III) atoms in complex **3** are given.

As illustrated in Figure 10a and 10b, there are two pairs of intramolecular hydrogen bond interactions (C0AA – H0AA···O23 and C29 – H29A···O21) and eight pairs of intermolecular hydrogen bond interactions (C4 – H4···O22, C10 – H10A···O7, C10 – H10B···O11, C14 – H14···O27, C22 – H22···O7, C23 – H23···O6, C32 – H32···O14 and C34 – H34···O3) in complex **3**. Besides, complex **3** visually shows a 3D perspective view (Figure 10c).

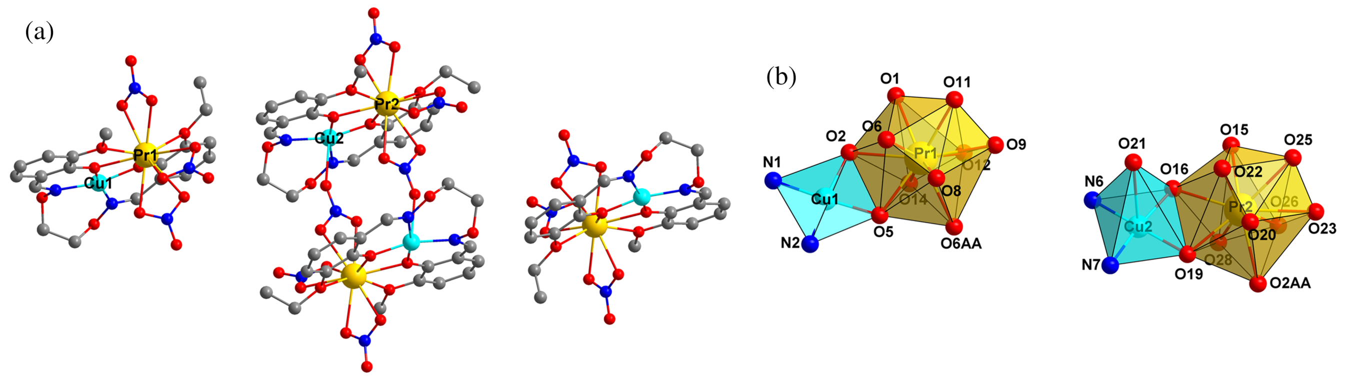

FIGURE 9 (a) Molecule structure of complex **3** (hydrogen atoms are omitted for clarity); (b) Coordination environments for Cu (II) and Pr (III) atoms

2.4.4 | Crystal structure of complex 4

X-ray crystallographic analysis indicates that the space group of complex **4** is a triclinic system of *P* − 1. Similar to the structure of complex **3**, it contains one neutral dimer $[Cu(L)Nd\ (NO_3)_3]_2$ unit and two independent and equivalent $[Cu(L)Nd\ (NO_3)_3]$ units (Figure 11a). As depicted in Figure 11b, in the independent $[Cu(L)Nd\ (NO_3)_3]$ units, the Cu (II) atoms (Cu2) are only surrounded by two nitrogen atoms (N6 and N7) and two

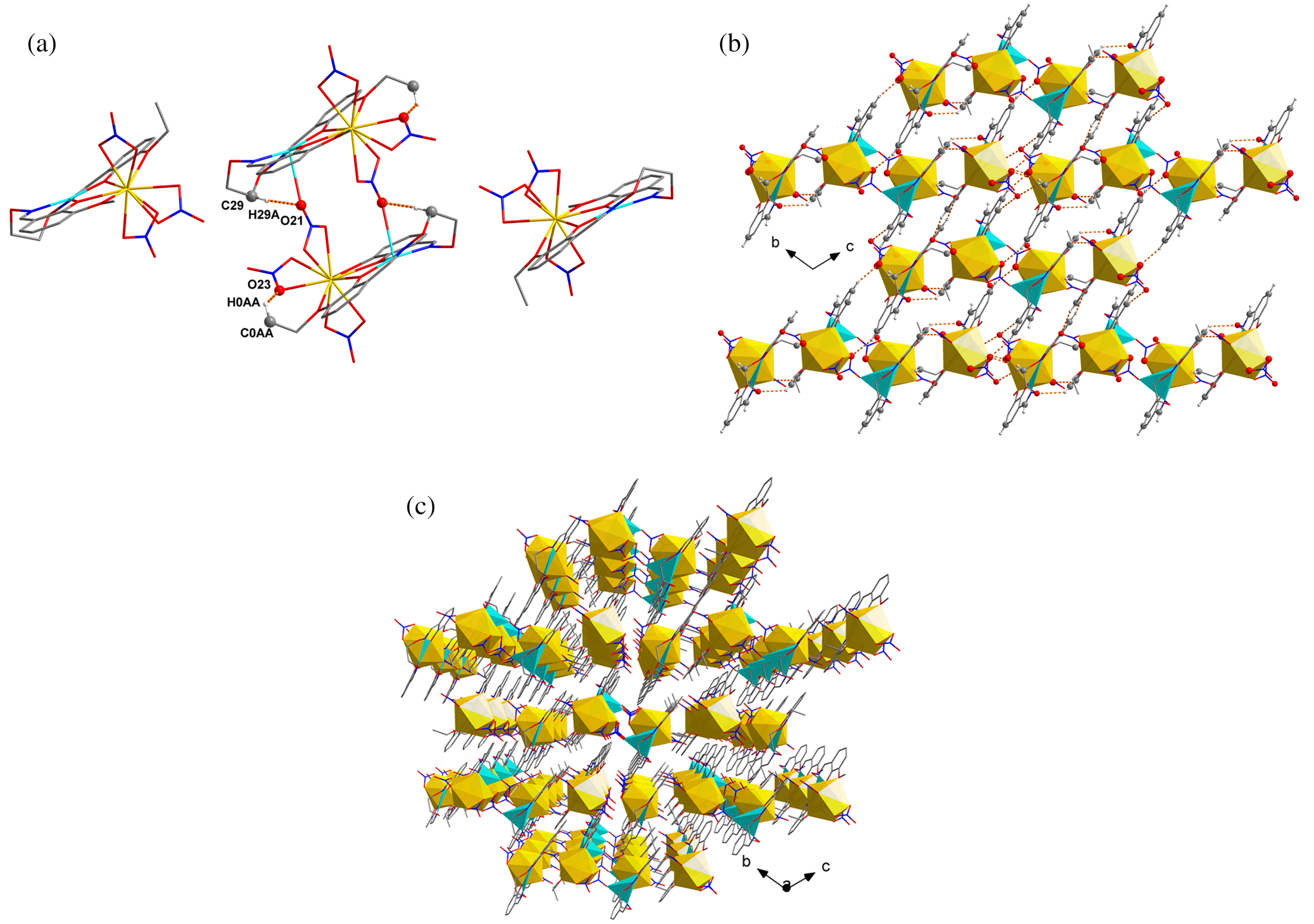

FIGURE 10 (a) View of the intramolecular hydrogen bonding interactions of complex **3**; (b) View of intermolecular hydrogen bonding interactions of complex **3** (hydrogen atoms, except those forming hydrogen bonds, are omitted for clarity); (c) View of the 3D intermolecular structure of complex **3**

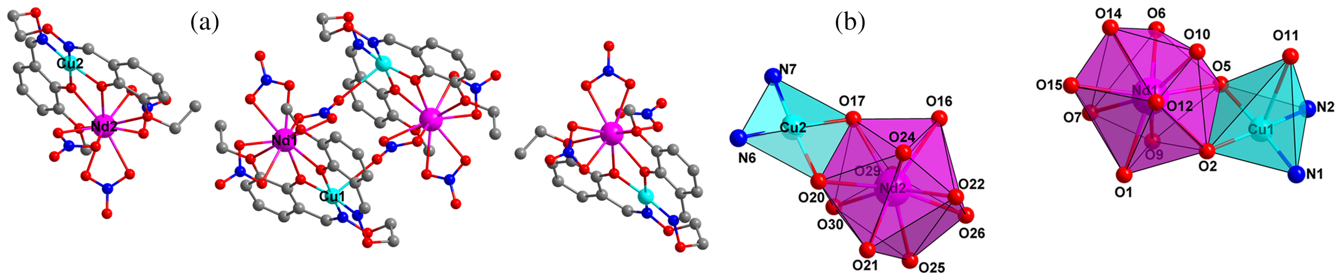

FIGURE 11 (a) Molecule structure of complex **4** (hydrogen atoms are omitted for clarity); (b) Coordination environments for Cu (II) and Nd (III) atoms

oxygen atoms (O17 and O20) in the ligand $(L)^{2-}$ units form a quadrilateral; in the neutral dimer $[Cu(L)Nd(NO_3)_3]$ unit, the Cu (II) atoms (Cu1) are surrounded by two nitrogen atoms (N1 and N2) and three oxygen atoms (O2, O5 and O11) from O_3N_2-donor environment to form a square pyramid geometric configuration (τ = 0.01716). Among them, two nitrogen atoms (N1 and N2) and two oxygen atoms (O2 and O5) serve as the equatorial plane, and one oxygen atom (O11) of the bidentate nitrate group occupies the apex of the square pyramid. The Nd (III) atoms (Nd1 and Nd2) in complex **4** are ten-coordinated, all of which also are composed of four oxygen atoms from the ligand $(L)^{2-}$ units and six oxygen atoms of three bidentate chelated nitrate groups, which assumes a distorted double tetragonal anti-prism geometry.

In complex **4**, four pairs of significant intramolecular hydrogen bonds (C9–H9A···O13, C9–H9B···O11, C36–H36B···O26 and C37–H37C···O15) are formed (Figure 12a). Meanwhile, complex **4** molecules forms a 2D supramolecular structure by intermolecular hydrogen bonds (C3–H3···O19, C5–H5···O24, C11–H11···O26, C14–H14···O30, C15–H15···O28, C19–H19B···O27,

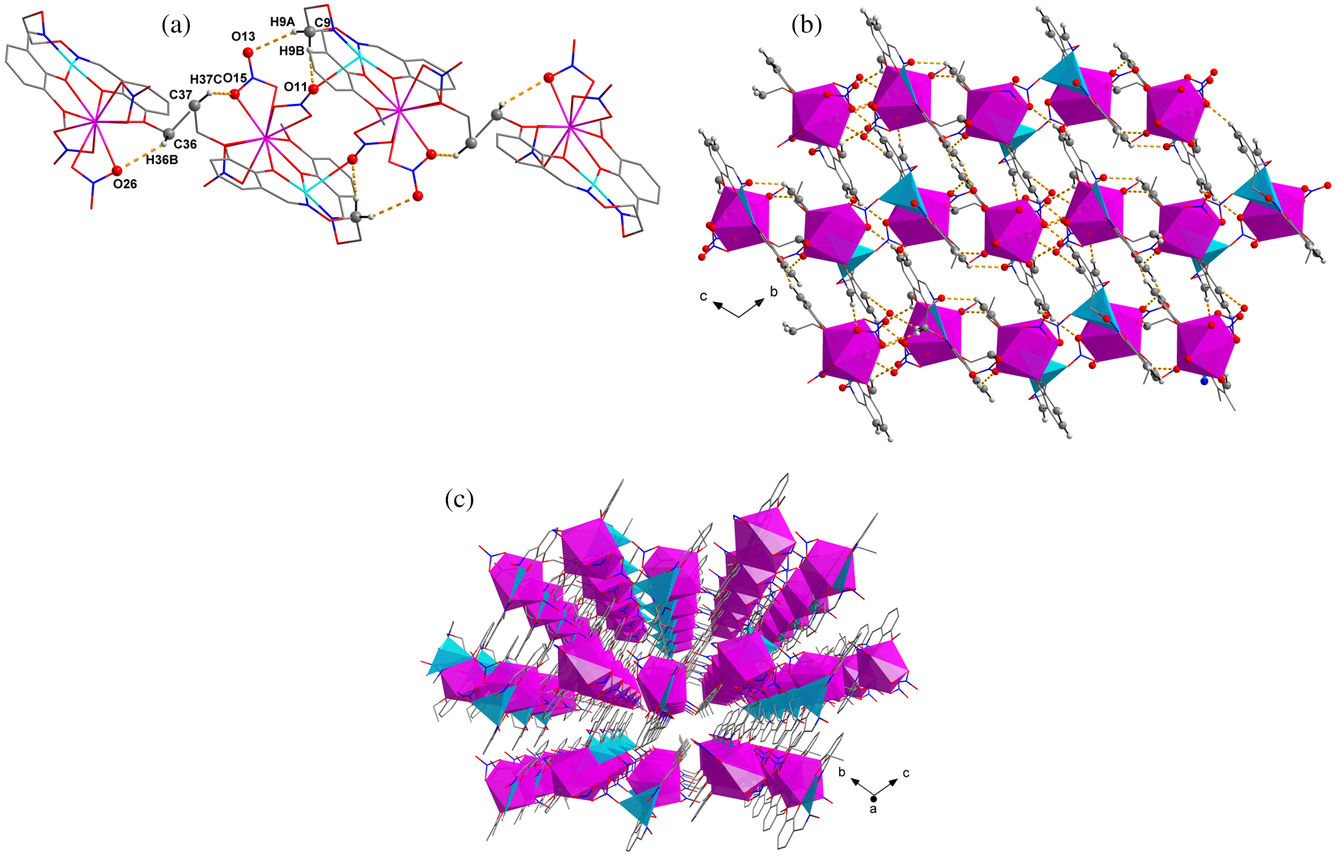

FIGURE 12 (a) View of the intramolecular hydrogen bonding interactions of complex **4**; (b) View of intermolecular hydrogen bonding interactions of complex **4** (hydrogen atoms, except those forming hydrogen bonds, are omitted for clarity); (c) View of the 3D intermolecular structure of complex **4**

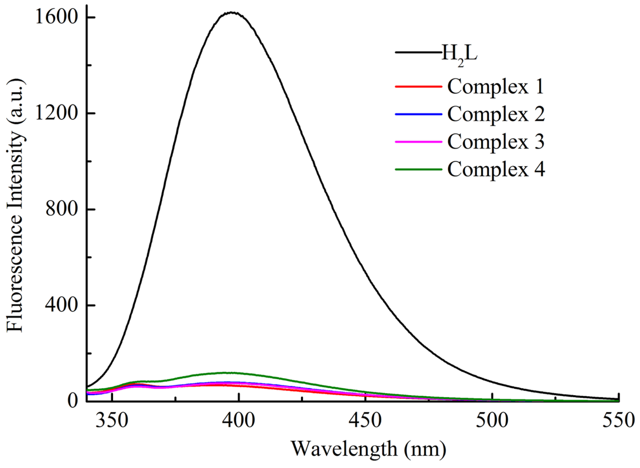

FIGURE 13 Fluorescence spectra of H_2L and its complexes **1–4**

C22–H22···O10, C23–H23···O13, C28–H28A···O28, C28–H28B···O25, C31–H31···O9 and C32–H32···O8) (Figure 12b). As depicted in Figure 12c, complex **4** visually shows a 3D perspective view.

2.5 | Spectroscopic studies

As shown in Figure 13, the fluorescence spectra of the ligand H_2L and its complexes **1–4** were excited at 320 nm. The emission spectrum of H_2L shows a wide emission band with a maximum emission peak at 395 nm, which is attributed to the π–π* electron transition in the ligand. Compared with H_2L, the fluorescence of complexes **1–4** is completely quenched, which may be due to LMCT emission, thus demonstrating the interaction of M (II/III) ions with the ligand $(L)^{2-}$ units. It is worth noting that complex **4** does not show Nd (III) characteristic emission peaks under this condition. It is possible that the intermediate $[(L)\text{–}Cu^{2+}]$ of the ligand H_2L and the metal Cu (II) ions suppressed Nd (III) light emission in the NIR region.[25]

2.6 | Antioxidant assay

The antioxidant radical performance of the complexes **1–4** was tested by riboflavin/methionine-NBT reduction method. If the complex has the activity of catalytic disproportionation of O_2•-, the effect of NBT and O_2•- can be suppressed. In other words, the ability of NBT to be reduced is inhibited. The absorbance A at different light time t with or without the addition of the complex is measured. A is plotted against t, the amount of change in absorbance over time can be obtained from the slope of the straight line in the figure, and the amount of change in absorbance over time before and after the addition of the complex is compared $\triangle_0$ and $\triangle$, the percentage f% of the NBT reduction reaction inhibited can be obtained (Equation 1).

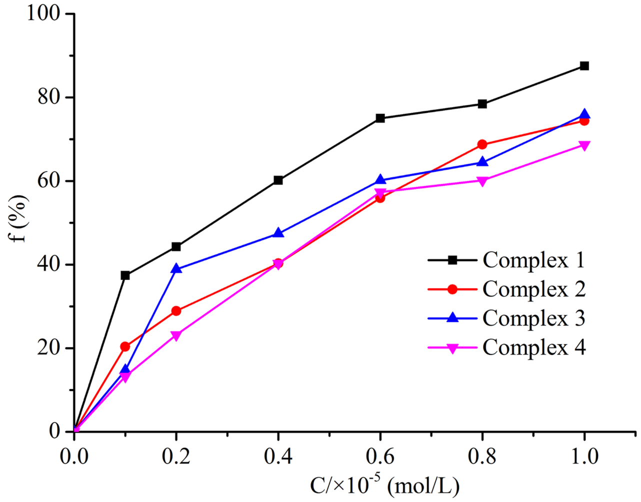

FIGURE 14 A plot of the scavenging percentage (%) vs. concentration of the complexes **1–4** on the superoxide radical

$$f\% = (\Delta_0 - \Delta)/\Delta_0 \times 100\% \tag{1}$$

Plot f% against Cm (concentration of complex) to get a curve, generally, the concentration of the active substance (Cm) with the inhibition percentage f% = 50% is taken as one SOD activity unit. IC50 is the concentration of antioxidants required to remove half of the free radicals in the antioxidant system.[58] If the IC50 value of the antioxidant is smaller, the concentration of the scavenger required to scavenge free radicals to 50% is lower, indicating that the better the scavenging effect of scavengers on free radicals.

As an important measurement method of antioxidant activity, the superoxide anion free radicals scavenging activity of the complex had been studied. As shown in Figure 14, the IC50 values of the four complexes are 0.2858×10^{-5} mol/l (**1**), 0.4383×10^{-5} mol/L (**2**), 0.5249×10^{-5} mol/l (**3**) and 0.5099×10^{-5} mol/l (**4**), the inhibition rate of the tested complex on O_2•- is **1** > **2** > **4** > **3**. Although the IC50 value of these complex is not as good as that of natural Cu, Zn-SOD (IC50 = 0.041 μmol/l) with strong oxidation resistance, but it is superior to the previously reported metal complexes.[59,60] Therefore, it can be considered that the four complexes have good scavenging activity for superoxide anion free radicals, and may be used as inhibitors for scavenging superoxide anion free radicals in the body, which requires us to further explore.

TABLE 3 Crystal data and the structure refinements for complexes **1–4**

Complex	1	2	3	4
Empirical formula	$C_{21}H_{28}LaN_5O_{17}Cu$	$C_{47}H_{68}Ce_2N_{10}O_{35}Cu_2$	$C_{76}H_{80}Pr_4N_{20}O_{60}Cu_4$	$C_{76}H_{80}Nd_4N_{20}O_{60}Cu_4$
Formula weight	824.93	1740.43	3051.40	3064.72
T (K)	273.15	273.15	273.15	173(2)
Wavelength (Å)	0.71073	0.71073	0.71073	0.71073
Crystal system	triclinic	monoclinic	triclinic	triclinic
Space group	*P*-1	*C*2/*c*	*P*-1	*P*-1
a (Å)	11.1869(2)	37.7323(10)	12.7428(3)	12.7041(12)
b (Å)	11.6946(2)	8.1155(2)	14.3572(3)	14.2621(14)
c (Å)	13.1950(3)	21.8290(5)	16.6826(4)	16.6252(17)
α (°)	70.0300(10)	90	106.0640(10)	106.041(2)
β (°)	81.1740(10)	92.9050(10)	111.2430(10)	111.043(2)
γ (°)	69.7340(10)	90	101.5210(10)	101.628(2)
V ($Å^3$)	1520.81(5)	6675.8(3)	2575.74(10)	2545.5(4)
Z	2	4	1	1
D_{calc} ($g\cdot cm^{-3}$)	1.801	1.732	1.967	1.999
μ (mm^{-1})	2.169	2.066	2.779	2.938
F (000)	822.0	3496.0	1508.0	1512.0
Crystal size (mm)	0.19 × 0.17 × 0.14	0.20 × 0.19 × 0.17	0.21 × 0.18 × 0.17	0.22 × 0.19 × 0.16
2θ Range (°)	4.988–52.04	6.312–52.044	5.328–52.034	4.802–50.016
Index ranges	$-13 \le h \le 13$ $-14 \le k \le 14$ $-16 \le l \le 16$	$-29 \le h \le 46$ $-10 \le k \le 10$ $-26 \le l \le 26$	$-15 \le h \le 15$ $-17 \le k \le 17$ $-20 \le l \le 20$	$-10 \le h \le 15$ $-16 \le k \le 16$ $-19 \le l \le 19$
Reflections collected Independent reflections	26,883 5,995 [$R_{int} = 0.0405$]	26,498 6,529 [$R_{int} = 0.0233$]	44,726 10,108 [$R_{int} = 0.0223$]	15,553 8,889 [$R_{int} = 0.0334$]
Completeness to θ	99.9% ($\theta = 25.242$)	99.3% ($\theta = 25.242$)	99.7% ($\theta = 25.242$)	99.1% ($\theta = 25.008$)
Data/restraints/parameters	5995/1/423	6529/1322/524	10,108/2851/874	8889/2263/731
GOF	1.027	1.047	1.106	1.042
Final R indexes [$I > 2\sigma(I)$]	0.0317, 0.0595	0.0254, 0.0680	0.0275, 0.0661	0.0722, 0.1712
Final R indexes [all data]	0.0499, 0.0663	0.0271, 0.0696	0.0305, 0.0677	0.0889, 0.1824
Largest diff. Peak and hole	0.58 and −0.38 e.$Å^{-3}$	0.77 and −0.52 e.$Å^{-3}$	0.59 and −0.72 e.$Å^{-3}$	4.16 and −4.49 e.$Å^{-3}$

SCHEME 1 Synthetic route of the ligand H_2L

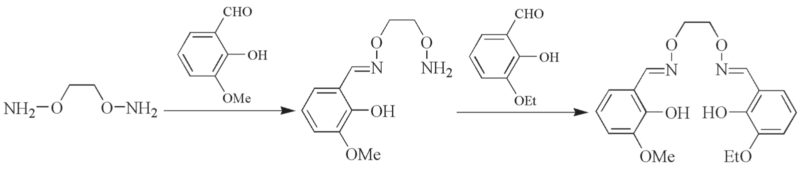

3 | CONCLUSIONS

In summary, an unsymmetric salamo-like ligand H_2L was synthesized and four heterobimetallic complexes were obtained by natural volatilization. These complexes were characterized by single crystal X-ray diffraction. Complex **1** is a hetero-dinuclear 3d–4f metal complex composed of [Cu(L)La $(NO_3)_2(\mu\text{-}NO_3)(H_2O)$] units and one crystalline ethanol molecule. Complex **2** is a hetero-tetranuclear 3d–4f metal complex consisting of one crystalline methanol molecule and two hetero-dinuclear [Cu(L)Ce $(NO_3)_2(\mu\text{-}NO_3)$ $(OAc)_2]_2$ units. Complexes **3** and **4** contain a neutral dimer [Cu(L)Ln $(NO_3)_3]_2$ unit and two independent and equivalent [Cu(L)Ln $(NO_3)_3$] units, forming a heteropolynuclear 3d–4f metal complexes. In addition, each molecule of complexes **1–4** is interconnected to form a three-dimensional supramolecular network structure, which indicates that complexes **1–4** are sufficiently stable, and still need further research on its potential application prospects. The measurement results of antioxidant activities of complexes **1–4** show that the inhibition rate of the tested complex on O_2•- is **1** > **2** > **4** > **3**. The 3d–4f metal complexes have many potential applications in the development of new therapeutic agents for diseases.

4 | EXPERIMENTAL

4.1 | Materials and measurements

All chemicals were obtained from commercial suppliers and used without further purification. X-ray single crystal structure for complexes **1–4** were measured and recorded using a Bruker APEX-II CCD surface inspection diffractometer (Bruker, Germany). Powder X-ray diffraction (PXRD) data were recorded on a Rigaku D/max-2,400 X-ray diffractometer with Cu-Kα as the radiation source (λ = 0.15406 nm) at room temperature. The ^1H NMR spectra were obtained by an AVANCE DRX-400/600 spectrometer with $CDCl_3$ as solvent (Bruker, Germany). The melting point of each substance was determined using a SGW X-4A Shanghai Jingke light micro melting point apparatus (Shanghai, China). Elemental analyses were performed a GmbH VariuoEL V3.00 automatic elemental analyzer (Berlin, Germany) and an IRIS ER/S-WP-1 ICP atomic emission spectrometer (Berlin, Germany). Infrared spectra were recorded on a Vertex 70 FT-IR spectrophotometer (Bruker, Germany) in the region 4,000–400 cm^{-1} using KBr pellets. Electronic absorption spectra in the UV–vis region were recorded with a UV-3900 spectrometer (Tokyo, Japan). Superoxide anion free radical was measured by UV-2550 Unico UV–Vis spectrophotometer (Shanghai, China).

4.2 | X-ray crystallography

All the intensity data for complexes **1–4** were collected on a Bruker APEX-II CCD diffractometer (Mo-Kα radiation and λ = 0.71073 Å) in Φ and ω scan modes. Use Olex 2 structure solution program[61] to solve the structures and refine all complexes. Structures were solved by direct methods followed by difference Fourier syntheses, and then refined by full-matrix least-squares techniques against F^2. All other non-hydrogen atoms were refined with anisotropic thermal parameters. Hydrogen atoms were placed in calculated positions and refined isotropically using a riding model. The crystals were kept at a certain temperature during data collection. CCDC 2000457 (for **1** at 273.15 K), 2,000,459 (for **2** at 273.15 K), 2,000,462 (for **3** at 273.15 K), and 2,000,458 (for **4** at 173.15 K) contain the supplementary crystallographic data for this paper. Table **3** lists the crystallographic data collection and refinement of all complexes.

4.3 | Synthesis of the H_2L

4.3.1 | Synthesis of 2-[*O*-(1-ethoxyamide)]oxime-6-methoxyphenol

To a stirred solution of 1, 2-bis (aminooxy)ethane (370.5 mg, 4.0 mmol) in ethanol solution (20 ml), 2-hydroxy-3-methoxybenzaldehye (300.8 mg, 2.0 mmol) was added, and the resulting mixture was refluxed for 5 hr at 45–55 °C. After vacuum distillation, the residue was purified by column chromatography with dichloromethane/ethyl acetate = 15/1 to obtain the intermediate product: 2-[*O*-(1-ethoxyamide)]oxime-6-methoxyphenol.[32] Yield: 65.6%. m.p: 93–94 °C. Anal. Calcd for $C_{10}H_{14}N_2O_4$ (%): C, 53.09; H, 6.24; N, 12.38. Found: C, 53.22; H, 6.11; N, 12.32.

4.3.2 | Synthesis of 6-methoxy-6′-ethoxy-2,2′-[ethylenedioxybis(nitrilomethylidyne)]diphenol (H_2L)

The ligand H_2L was synthesized according to the literature (Scheme **1**),[47] which was prepared by refluxing a mixture of the obtained above 2-[*O*-(1-ethoxyamide)]oxime-6-methoxyphenol (455.0 mg, 2.0 mmol) and 3-ethoxysalicylaldehyde (330.5 mg, 2.0 mmol) in ethanol (70 ml). The reaction mixture was heated to *ca.* 55 °C reflux for 6 hr and the resulting white solid product was filtered off, washed successively with few amounts of n-hexane, and finally dried in air. Yield: 82.5%. m.p: 100–101 °C. Anal. Calcd for $C_{19}H_{22}N_2O_6$ (%): C, 60.95; H, 5.92; N, 7.48. Found: C, 61.02; H, 5.89; N, 7.41. ^1H NMR (400 MHz, $CDCl_3$) δ 9.73 (s, 1H, –OH), 9.69 (s, 1H, –OH), 8.26 (s, 2H, –N=CH), 6.95–6.79 (m, *J* = 20, 12 Hz, 6H, –ArH), 4.47 (s, 4H, –CH_2), 4.11 (s, 2H, –OCH_2), 3.91 (s, 3H, –OCH_3), 1.48 (s, 3H, –CH_3). IR (KBr, cm^{-1}): 3427 (vs), 2,978 (w), 2,930 (m), 2,876 (w), 2,835 (w), 2073 (m), 1,613 (vs), 1,468 (s), 1,420 (w), 1,386 (w), 1,352 (m), 1,250 (vs), 1,059 (vs), 985 (m), 733 (m), 638 (s) and 488 (m). UV–Vis (CH_3CH_2OH), λ_{max} (nm) [(ε_{max}): (dm^3 mol^{-1} cm^{-1})]: 270 and 319 nm (1.0×10^{-5} M).

4.4 | Synthesis of the complexes 1–4

4.4.1 | Synthesis of [cu(L)La $(NO_3)_2$ (μ-NO_3)(H_2O)]·EtOH (1)

To a stirred solution of H_2L (7.62 mg, 0.2 mmol) in dichloromethane (2 ml) were added Cu $(OAc)_2{\cdot}H_2O$ (4.08 mg, 0.2 mmol) in absolute EtOH (3 ml) and a solution of La $(NO_3)_3{\cdot}6H_2O$ (8.74 mg, 0.2 mmol) in absolute EtOH (3 ml), respectively. The resulting mixture was stirred for several tens of minutes, then the dark green solution was filtered and sealed. The brownish green bulk crystal product **1** was obtained in a few weeks. For **1**: $C_{21}H_{28}LaN_5O_{17}Cu$, yield 8.9 mg, 44.5%. Elemental analysis: Anal. calc. (%): C, 30.58; H, 3.42; N, 8.49; Cu, 7.70; La, 16.84. Found (%): C, 30.75; H, 3.48; N, 8.43; Cu, 7.81; La, 16.60.

4.4.2 | Synthesis of [cu(L)Ce $(NO_3)_2$(μ-NO_3)$(OAc)_2$$]_2$·MeOH (2)

The synthesis process of complex **2** is similar to that of complex **1**. To a stirred solution of H_2L (7.56 mg, 0.2 mmol) in dichloromethane (2 ml) were added Cu $(OAc)_2{\cdot}H_2O$ (4.29 mg, 0.2 mmol) in absolute MeOH (3 ml) and a solution of Ce $(NO_3)_3{\cdot}6H_2O$ (8.88 mg, 0.2 mmol) in absolute MeOH (3 ml), respectively. For **2**: $C_{47}H_{68}Ce_2N_{10}O_{35}Cu_2$, yield 9.2 mg, 46.0%. Elemental analysis: Anal. calc. (%): C, 32.44; H, 3.94; N, 8.05; Cu, 7.30; Ce, 16.10. Found (%): C, 32.62; H, 3.98; N, 7.99; Cu, 7.39; Ce, 15.91.

4.4.3 | Synthesis of [{cu(L)Pr $(NO_3)_3\}_2$] [cu(L)Pr $(NO_3)_3]_2$ (3)

The synthesis process of complex **3** is completely the same as the method and process of complex **1**, except that Pr $(NO_3)_3{\cdot}6H_2O$ (8.95 mg, 0.2 mmol) was used instead of La $(NO_3)_3{\cdot}6H_2O$ (8.74 mg, 0.2 mmol). For **3**: $C_{76}H_{80}Pr_4N_{20}O_{60}Cu_4$, yield 8.3 mg, 40.6%. Elemental analysis: Anal. calc. (%): C, 29.91; H, 2.64; N, 9.18; Cu, 8.33; Pr, 18.47. Found (%): C, 30.12; H, 2.51; N, 9.13; Cu, 8.37; Pr, 18.36.

4.4.4 | Synthesis of [{cu(L)Nd $(NO_3)_3\}_2$] [cu(L)Nd $(NO_3)_3]_2$ (4)

The synthesis process of complex **4** is completely the same as the method and process of complex **1**, except that Nd $(NO_3)_3{\cdot}6H_2O$ (8.01 mg, 0.2 mmol) was used instead of La $(NO_3)_3{\cdot}6H_2O$ (8.74 mg, 0.2 mmol). For **4**: $C_{76}H_{80}Nd_4N_{20}O_{60}Cu_4$, yield 7.8 mg, 38.2%. Elemental analysis: Anal. calc. (%): C, 29.78; H, 2.63; N, 9.14; Cu, 8.29; Nd, 18.83. Found (%): C, 29.97; H, 2.68; N, 9.03; Cu, 8.38; Nd, 18.66.

FUNDING

This work was supported by the National Natural Science Foundation of China (21761018), Science and Technology Program of Gansu Province (18YF1GA057) and the Program for Excellent Team of Scientific Research in Lanzhou Jiaotong University (201706), which are gratefully acknowledged.

AUTHOR CONTRIBUTIONS

Xiao-Xin An: Investigation. **Chang Liu:** Data curation; software. **Hai-Tao Long:** Data curation; formal analysis.

Data Availability Statement

The data that supports the findings of this study are available in the supplementary material of this article.

ORCID

Li Zhao https://orcid.org/0000-0003-3922-213X

REFERENCES

[1] L. Wang, Z. L. Wei, C. Liu, W. K. Dong, J. X. Ru, *Spectrochim. Acta A* **2020**, *239*, 118496.

[2] J. Chang, H. J. Zhang, H. R. Jia, Y. X. Sun, *Chin. J. Inorg. Chem.* **2018**, *34*, 2097.

[3] X. Y. Dong, Q. Zhao, Q. P. Kang, X. Y. Li, W. K. Dong, *Crystals* **2018**, *8*, 230.

[4] Y. X. Sun, Y. Q. Pan, X. Xu, Y. Zhang, *Crystals* **2019**, *9*, 607.

[5] S. Z. Zhang, J. Chang, H. J. Zhang, Y. X. Sun, Y. Wu, Y. B. Wang, *Chin. J. Inorg. Chem.* **2020**, *36*, 503.

[6] J. Li, H. J. Zhang, J. Chang, Y. X. Sun, Y. Q. Huang, *Crystals* **2018**, *8*, 176.

[7] L. W. Zhang, X. Y. Li, Q. P. Kang, L. Z. Liu, J. C. Ma, W. K. Dong, *Crystals* **2018**, *8*, 173.

[8] H. R. Jia, J. Chang, H. J. Zhang, J. Li, Y. X. Sun, *Crystals* **2018**, *8*, 272.

[9] X. X. An, Q. Zhao, H. R. Mu, W. K. Dong, *Crystals* **2019**, *9*, 101.

[10] L. W. Zhang, Y. Zhang, Y. F. Cui, M. Yu, W. K. Dong, *Inorg. Chim. Acta* **2020**, *506*, 119534.

[11] L. W. Zhang, L. Z. Liu, F. Wang, W. K. Dong, *Molecules* **2018**, *23*, 1141.

[12] S. Akine, T. Taniguchi, W. K. Dong, S. Masubuchi, T. Nabeshima, *J. Org. Chem.* **2005**, *70*, 1704.

[13] X. Q. Song, Y. J. Peng, G. Q. Chen, X. R. Wang, P. P. Liu, W. Y. Xu, *Inorg. Chim. Acta* **2015**, *427*, 13.

[14] X. Q. Song, Y. Q. Peng, G. Q. Chen, X. R. Wang, P. P. Liu, *Inorg. Chim. Acta* **2015**, *427*, 13.

[15] L. Q. Chai, Q. Hu, K. Y. Zhang, L. C. Chen, Y. X. Li, H. S. Zhang, *Appl. Organomet. Chem.* **2018**, *32*, e4426.

[16] L. Q. Chai, L. Zhou, K. Y. Zhang, H. S. Zhang, *Appl. Organomet. Chem.* **2018**, *32*, e4576.

[17] Z. L. Ren, J. Hao, P. Hao, X. Y. Dong, Y. Bai, W. K. Dong, *Z. Naturforsch B* **2018**, *73*, 203.

[18] L. Q. Chai, L. J. Tang, K. Y. Zhang, J. Y. Zhang, H. S. Zhang, *Appl. Organomet. Chem.* **2017**, *31*, e3786.

[19] J. Hao, X. Y. Li, Y. Zhang, W. K. Dong, *Materials* **2018**, *11*, 523.

[20] L. Zhou, Q. Hu, L. Q. Chai, K. H. Mao, H. S. Zhang, *Polyhedron* **2019**, *158*, 102.

[21] Y. Zhang, L. Z. Liu, Y. D. Peng, N. Li, W. K. Dong, *Transition Met. Chem.* **2019**, *44*, 627.

[22] Q. P. Kang, X. Y. Li, Q. Zhao, J. C. Ma, W. K. Dong, *Appl. Organomet. Chem.* **2018**, *32*, e4379.

[23] L. Wang, Z. L. Wei, Z. Z. Chen, C. Liu, W. K. Dong, Y. J. Ding, *Microchem. J.* **2020**, *155*, 104801.

[24] L. H. Li, W. K. Dong, Y. Zhang, S. F. Akogun, L. Xu, *Appl. Organomet. Chem.* **2017**, *31*, e3818.

[25] X. Y. Li, Q. P. Kang, C. Liu, Y. Zhang, W. K. Dong, *New J. Chem.* **2019**, *43*, 4605.

[26] T. K. Chin, S. Endud, S. Jamil, S. Budagumpi, H. O. Lintang, *Catal. Lett.* **2013**, *143*, 282.

[27] X. Q. Song, P. P. Liu, C. Y. Wang, Y. A. Liu, W. S. Liu, M. Zhang, *RSC Adv.* **2017**, *7*, 22692.

[28] P. P. Liu, C. Y. Wang, M. Zhang, X. Q. Song, *Polyhedron* **2017**, *129*, 133.

[29] X. Q. Song, P. P. Liu, Y. A. Liu, J. J. Zhou, X. L. Wang, *Dalton Trans.* **2016**, *45*, 8154.

[30] X. Q. Song, C. Y. Wang, H. H. Meng, A. A. A. Shamshoom, W. S. Liu, *Inorg. Chem.* **2018**, *57*, 10873.

[31] T. Yamaguchi, J. P. Costes, Y. Kishima, M. Kojima, Y. Sunatsuki, N. Bréfuel, J. P. Tuchagues, L. Vendier, W. Wernsdorfer, *Inorg. Chem.* **2010**, *49*, 9125.

[32] Y. Zhang, M. Yu, Y. Q. Pan, Y. Zhang, L. Xu, X. Y. Dong, *Appl. Organomet. Chem.* **2020**, *34*, e5442.

[33] C. Liu, X. X. An, Y. F. Cui, K. F. Xie, W. K. Dong, *Appl. Organomet. Chem.* **2020**, *34*, e5272.

[34] Y. Q. Pan, Y. Zhang, M. Yu, Y. Zhang, L. Wang, *Appl. Organomet. Chem.* **2020**, *34*, e5441.

[35] Z. L. Wei, L. Wang, J. F. Wang, W. T. Guo, Y. Zhang, W. K. Dong, *Spectrochim. Acta A* **2020**, *228*, 117775.

[36] Y. Q. Pan, X. Xu, Y. Zhang, Y. Zhang, W. K. Dong, *Spectrochim. Acta A* **2020**, *229*, 117927.

[37] H. R. Mu, M. Yu, L. Wang, Y. Zhang, Y. J. Ding, *Phosphorus, Sulfur Silicon Relat. Elem.* **2020**, *195*, 730.

[38] F. Wang, L. Z. Liu, L. Gao, W. K. Dong, *Spectrochim. Acta A* **2018**, *203*, 56.

[39] L. Z. Liu, L. Wang, M. Yu, Q. Zhao, Y. Zhang, Y. X. Sun, W. K. Dong, *Spectrochim. Acta A* **2019**, *222*, 117209.

[40] C. Liu, Z. L. Wei, H. R. Mu, W. K. Dong, Y. J. Ding, *J. Photochem. Photobio. A* **2020**, *397*, 112569.

[41] Q. P. Kang, X. Y. Li, L. Wang, Y. Zhang, W. K. Dong, *Appl. Organomet. Chem.* **2019**, *33*, e5013.

[42] Q. P. Kang, X. Y. Li, Z. L. Wei, Y. Zhang, W. K. Dong, *Polyhedron* **2019**, *165*, 38.

[43] Q. Zhao, X. X. An, L. Z. Liu, W. K. Dong, *Inorg. Chim. Acta* **2019**, *490*, 6.

[44] L. Z. Liu, M. Yu, X. Y. Li, Q. P. Kang, W. K. Dong, *Chin. J. Inorg. Chem.* **2019**, *35*, 1283.

[45] H. R. Mu, X. X. An, C. Liu, Y. Zhang, W. K. Dong, *J. Struct. Chem.* **2020**, *61*, 1218.

[46] J. Chang, S. Z. Zhang, Y. Wu, H. J. Zhang, Y. X. Sun, *Transition Met. Chem.* **2020**, *45*, 279.

[47] L. Wang, Y. Q. Pan, J. F. Wang, Y. Zhang, Y. J. Ding, *J. Photochem. Photobio. A* **2020**, *400*, 112719.

[48] L. Q. Chai, Y. X. Li, L. C. Chen, J. Y. Zhang, J. J. Huang, *Inorg. Chim. Acta* **2016**, *444*, 193.

[49] H. L. Wu, Y. C. Bai, Y. H. Zhang, Z. Li, M. C. Wu, C. Y. Chen, J. W. Zhang, *J. Coord. Chem.* **2014**, *67*, 3054.

[50] H. L. Wu, G. L. Pan, Y. C. Bai, *J. Chem. Res.* **2014**, *38*, 211.

[51] H. L. Wu, Y. C. Bai, Y. H. Zhang, G. L. Pan, J. Kong, F. Shi, X. L. Wang, *Z. Anorg. Allg. Chem.* **2014**, *640*, 2062.

[52] M. Yu, Y. Zhang, Y. Q. Pan, L. Wang, *Inorg. Chim. Acta* **2020**, *509*, 119701.

[53] X. X. An, Z. Z. Chen, H. R. Mu, L. Zhao, *Inorg. Chim. Acta* **2020**, *511*, 119823.

[54] X. Y. Dong, Q. P. Kang, X. Y. Li, J. C. Ma, W. K. Dong, *Crystals* **2018**, *8*, 139.

[55] Y. D. Peng, F. Wang, L. Gao, W. K. Dong, *J. Chin. Chem. Soc.* **2018**, *65*, 893.

[56] X. Y. Dong, Q. Zhao, Z. L. Wei, H. R. Mu, H. Zhang, W. K. Dong, *Molecules* **2018**, *23*, 1006.

[57] H. J. Zhang, J. Chang, H. R. Jia, Y. X. Sun, *Chin. J. Inorg. Chem.* **2018**, *34*, 2261.

[58] Y. V. Yuan, D. E. Bone, M. F. Carrington, *Food Chem.* **2005**, *91*, 485.

[59] H. L. Wu, L. X. Xia, Y. Qu, K. Zhao, C. Wang, Y. C. Wu, *Appl. Organomet. Chem.* **2019**, e5297.

[60] S. S. Mao, K. S. Shen, X. K. Shi, H. L. Wu, X. T. Han, C. Li, G. Z. Huang, *Inorg. Chim. Acta* **2018**, *471*, 82.

[61] O. V. Dolomanov, L. J. Bourhis, R. J. Gildea, J. A. K. Howard, H. Puschmann, *J. Appl. Crystallogr.* **2009**, *42*, 339.

SUPPORTING INFORMATION

Additional supporting information may be found online in the Supporting Information section at the end of this article.

How to cite this article: Pu L-M, An X-X, Liu C, Long H-T, Zhao L. Insights into crystal structures, supramolecular architectures and antioxidant activities of self-assembled fluorescent hetero-multinuclear [Cu (II)-Ln (III)] (Ln = La, Ce, Pr and Nd) salamo-like complexes. *Appl Organomet Chem*. 2020;e5980. https://doi.org/10.1002/aoc.5980